Shape and Thermodynamic Stability of Pyrite FeS2 Nanocrystals and Nanorods

ARTICLE *in* THE JOURNAL OF PHYSICAL CHEMISTRY C · JULY 2007

Impact Factor: 4.77 · DOI: 10.1021/jp0738199

2 AUTHORS:

Amanda S Barnard
The Commonwealth Scientific and Industrial …
181 PUBLICATIONS **4,316** CITATIONS
SEE PROFILE

Salvy P Russo
RMIT University
167 PUBLICATIONS **2,268** CITATIONS
SEE PROFILE

Shape and Thermodynamic Stability of Pyrite FeS_2 Nanocrystals and Nanorods

A. S. Barnard*,† and S. P. Russo‡

Department of Materials, University of Oxford, Oxford, OX1 3PH, United Kingdom, and Applied Physics, School of Applied Sciences, RMIT University, Melbourne, 3001, Australia

Received: May 17, 2007; In Final Form: June 11, 2007

The pyrite polymorph of iron disulfide (FeS_2) has been attracting considerable attention, as it shows promise for solar energy conversion devices, solid-state batteries, and catalysis. As-prepared FeS_2 powders naturally displayed rod-like morphologies, but if tailor-made pyrite nanocrystals and nanorods are to be reliably exploited in future devices, it is desirable to be able to predict and precisely control the shape (and aspect ratio) of FeS_2, and to understand the morphological stability under various conditions. Therefore, we have begun by investigating the relationship between size, shape, axial orientations, and aspect ratio of unpassivated FeS_2 nanostructures, using a thermodynamic model and energetic parameters calculated from first principles. The results show that the unusual morphologies such as the decahedral pyritohedron are less likely at the nanoscale than they are macroscopically, and that the preferred orientation of 1-D FeS_2 nanostructures is likely to be defined by kinetics, irrespective of aspect ratio.

1. Introduction

The industrial and economic importance of metal sulfide materials has increased in recent years, owing to their wide range of physical, electronic, and chemical properties which are under investigation for a range of possible applications including solar cells,[1−3] solid-state batteries,[4] and catalysis. The pyrite polymorph of iron disulfide (FeS_2) is of particular interest, and shows promise for solar energy conversion devices in both photoelectrochemical and photovoltaic solar cells[5] and solid state solar cells[6] due to its favorable solid-state properties.[2,3,7−9]

The structure of pyrite FeS_2 is cubic ($Pa\bar{3}$), where the anions of a NaCl lattice are replaced by S_2 dimers with their molecular axes orientated along the four crystallographic ⟨111⟩ directions. Each S atom is bound to another S atom and three Fe atoms, so that each Fe atom is coordinated to six S atoms with equal Fe−S bond distances. Experimentally, FeS_2 is diamagnetic with the metal ions in a low-spin Fe^{2+} configuration. First principles calculations of the lowest energy electronic structure (with the Fe^{2+} ions converged in the low-spin states) have revealed that the electronic properties of FeS_2 may be sensitive to changes in stoichiometry that result from different synthesis techniques.[10] In general, a variety of methods are used to produce polycrystalline and single-crystal pyrite, including metal organic chemical vapor deposition MOCVD[11] or by mixing ironpentacarbonyl and sulfur or hydrogen sulfide in an organic solvent.[12] Like natural crystals, these synthetic samples are often found to be sulfur deficient, with a FeS_{2-x} composition ($0.05 < x < 0.25$).[13]

In addition to controlling variations in composition and stoichiometry, over the past decade the attention of the synthesis community has expanded to included the preparation of a variety of low-dimensional materials with controlled morphologies. In particular, one-dimensional (1-D) semiconductor nanomaterials have attracted considerable interest because of their fundamental physical, chemical, optical, electrical, and magnetic properties which are distinct from their bulk counterparts, giving rise to potential applications in nanoscale devices.[14−18] Although there are several reports on different 1-D semiconducting sulfide nanostructures,[19−24] such as CdS nanorods, nanowires, nanoribbons, and nanotubes with the hexagonal (wurtzite) structure, cubic structures such as pyrite FeS_2 have been the subject of comparatively fewer studies. Nevertheless, 1-D FeS_2 nanostructures have been successfully prepared,[25] via a solvothermal process at 130 °C in ethylenediamine, akin to the hydrothermal process in water. Ethylenediamine is useful in this type of experiment, since its chelating property has been shown to induce 1-D growth.[27] The as-prepared FeS_2 powders naturally displayed a rod-like morphology, with diameters of 20−50 nm and lengths of up to 1000 nm. In this case the morphology of the particles was controlled by varying the solvent, although the final nanorods were nonuniform in length.[25] More recently, sulfur-deficient iron pyrrhotite ($Fe_{1-x}S$) nanowires were reported by Nath et el.,[26] and the first successful synthesis of large quantities of FeS_2 nanoparticles, nanowires, nanoribbons, and nanotubes was reported by Kar and Chaudhuri.[28,29] Like previous studies, these structures were also produced via a solvothermal process, at relatively low temperature, and using ethylenediamine as the solvent, suggesting this may be a route toward the ultimate goal of morphological controlled synthesis.[30] It has already been established that replacing ethylenediamine with benzene promotes more quasispherical shapes.[25]

However, if tailor-made pyrite FeS_2 nanocrystals and nanorods are to be reliably exploited in future devices, and it is desirable to be able to predict the equilibrium shape (and aspect ratio) of FeS_2 under various conditions, and to gain some appreciation of the metastability of kinetically driven shapes with respect to possible morphological transformations. This is particularly interesting when one considers the occurrence of perfect cubic morphologies and unusual decahedral morphologies (with pentagonal facets) known as "pyritohedrons" at the macroscale, neither of which are thermodynamically favored. It is unclear as to whether these shapes will be stable or unstable

* Address correspondence to this author. E-mail: amanda.barnard@materials.ox.ac.uk.
† University of Oxford.
‡ RMIT University.

10.1021/jp0738199 CCC: $37.00
Published on Web 07/18/2007

at the nanoscale, just as it is unknown whether there is a preferred axial orientation and shape for pyrite nanorods. Investigations of this sort are ideal problems for theoretical modeling, where the shape-stability as a function of size or surface chemistry may be tested systemically. We have begun this task by first investigating the relationship between size, shape, axial orientations, and aspect ratio of unpassivated pyrite FeS_2 nanostructures.

2. Theoretical Method

This has been done by using a shape-dependent thermodynamic model based on a geometric summation of the Gibbs free energy,[31] which has been successfully used to examine the shape of oxides[32,33] and semiconductors[34] in the past. A truncated version of the model has been used here, which is applicable specifically to isolated, defect-free structures in the range ~3−100 nm, as described in ref 35. In this version the total free energy G is described in terms of the specific surface free energies γ_i, for facts i, weighted by the factors f_i (such that $\sum_i f_i = 1$):

$$G = \Delta G_f^o + \frac{M}{\rho}\left(1 - \frac{2\sum_i f_i\sigma_i}{B_0 R} + \frac{P_{ex}}{B_0}\right)[q\sum_i f_i\gamma_i] \qquad (1)$$

where M is the molar mass, ρ is the density, and the volume dilation induced by the isotropic surface stresses σ_i and external pressure P_{ex} is included by using the Laplace−Young formalism, as defined in ref 35. In all cases we have assumed atmospheric external pressure.

The parametrization of this model for pyrite FeS_2 has been undertaken from first principles, using Density Functional Theory (DFT) within the Generalized-Gradient Approximation (GGA) with the Perdew and Wang (PW91)[36] exchange-correlation functional, implemented via the Vienna Ab initio Simulation Package (VASP).[37,38] We have used the Linear Tetrahedron Method (LTM) and ultrasoft, gradient-corrected Vanderbilt-type pseudopotentials (US-PP)[39,40] for both the initial structural relaxations and reconstructions, and the final static (single point) calculations required for the determination of the specific surface free energies and surface stress tensors. The electronic relaxation technique used here is an efficient matrix-diagonalization routine based on a sequential band-by-band residual minimization method of single-electron energies,[41,42] with direct inversion in the iterative subspace, whereas the ionic relaxation involves minimization of the Hellmann−Feynman forces, to an energy convergence of 10^{-4} eV.

Using these computational methods we obtain lattice constants of $a = 5.4259$ Å and $u_s = 0.3830$ Å, which are in excellent agreement with the values of $a = 5.360$ Å and $u_s = 0.384$ Å calculated by using a similar method by Raybaud et al.[43] and the values of $a = 5.520$ Å and $u_s = 0.380$ Å calculated by Muscat et al.,[10] as well as the values of $a = 5.416$ Å and $u_s = 0.385$ Å measured experimentally.[44] Similarly, the bulk modulus $B_0 = 154.89$ GPa and derivative $B' = 4.69$ calculated by using the Birch Murnaghan equation of state[45] are in good agreement with the values of $B_0 = 164$ GPa and $B' = 3.5$ calculated by Muscat et al.,[10] and the corresponding experimental values.[46−48]

The remaining parameters required for the Gibbs free energy summation are the specific surface free energies and the isotropic surface stresses. In the present study we have calculated these values for the {100}, {111}, {110}, and {210} surfaces, using the same computational method described above. In each case a two-dimensional slab was generated, surrounded by 10 Å of vacuum space perpendicular to the crystallographic plane of interest. Each slab consisted of supercells containing 32 molecular units (96 atoms), and the surface structure and internal parameters were fully reconstructed and relaxed prior to the calculation of the energy and stress. The specific surface free energies γ_i were calculated in the standard way as describe in ref 49, and the isotropic surfaces stresses σ_i were computed from the trace of the surface stress tensor. The resulting values of $\gamma_{(100)} = 1.05$ J·m^{-2}, $\gamma_{(111)} = 1.29$ J·m^{-2}, $\gamma_{(110)} = 1.60$ J·m^{-2}, and $\gamma_{(210)} = 1.48$ J·m^{-2} are slightly lower than (but otherwise in excellent agreement with) the values of 1.06 J·m^{-2}, 1.40 J·m^{-2}, 1.68 J·m^{-2}, and 1.54 J·m^{-2} calculated by Hung et al., respectively, using comparable theoretical methods.[50,51] No previous results could be located for comparison with the calculated values of $\sigma_{(100)} = 0.14$ J·m^{-2}, $\sigma_{(111)} = 1.44$ J·m^{-2}, $\sigma_{(110)} = -0.24$ J·m^{-2}, and $\sigma_{(210)} = -1.04$ J·m^{-2}. This being said, these values are reasonable when one considers the direction and magnitude of the surface layer relaxation (perpendicular to the plane of the surface) and the degree of surface reconstructions of the surface of the slabs used here, and those reported in refs 50 and 51.

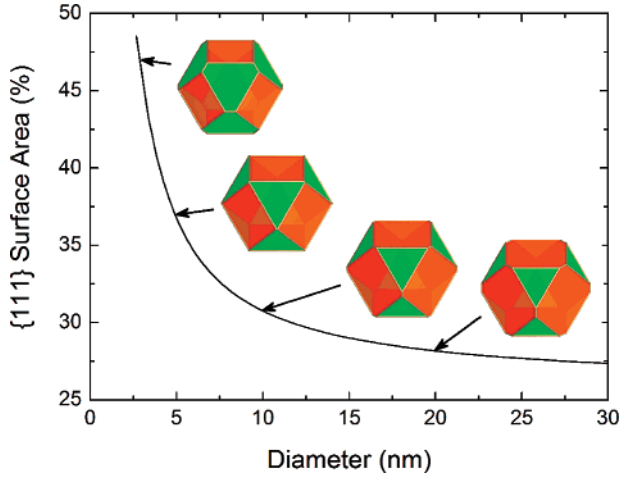

Figure 1. Equilibrium shape of pyrite FeS_2 nanocrystals, defined in terms of the fraction of {111} surface area. Schematic representations of the shapes are shown for nanocrystal 3, 5, 10, and 20 nm in diameter (left to right). {100} facets are shown in red, and {111} facets are shown in green.

It is important to point out that these quantities were calculated at zero temperature. This means that G is effectively a free energy of formation that is equivalent to the enthalpy for formation, but it also has implications for the applicability of the model results to real experiments. Our model results are more related to low-temperature quasiequilibrium conditions, and consequently have limited applicability to cases where pyrite FeS_2 nanostructures are grown at high temperature.

3. Discussion of Results

3.1. Nanocrystals. By using the expression given in eq 1, and the set of values for a, B_0, γ_i, and σ_i listed above, the predicted equilibrium shape of a pyrite nanocrystal over a range of diameters is show in Figure 1. First, we can see that the equilibrium shape consists of {100} and {111} facets, but no {110} and {210} facets, which is consistent with the morphology predicted by the Wulff construction for pyrite macrocrystals. These shapes are effectively cubes that have been truncated (to varying degrees) in the ⟨111⟩ directions, resulting in shapes occupying the cuboctahedron-truncated cube shape-continuum. However, the Wulff construction does not take into account the

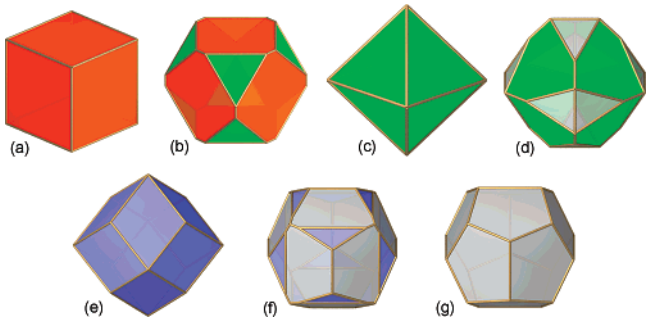

Figure 2. A collection of shapes for pyrite FeS_2 nanocrystals, formed using limited combinations of crystallographic forms: (a) cube, (b) optimized truncated cubic shape, (c) octahedron, (d) modified octahedron, (e) rhombic dodecahedron, (f) modified pyritohedron, and (g) pyritohedron. {100} facets are shown in red, {111} facets in green, {110} facets in blue, and {210} facets in gray.

desire for nanocrystals to minimize the total surface stress and the surface-to-volume ratio q (as well as the total surface energy), and it is possible that the morphologies of nanocrystals may deviate from the Wulff shape.

Beyond the changes in shape one may expect by introducing the surface stresses σ_i, a variation in shape will naturally alter the values of f_i and q, by amounts Δf_i and Δq, respectively. The introduction (or increase in size) of a higher energy facet will result in Δf_{high} being positive, and Δf_{low} being negative. This combination will naturally increase the total value of $\sum_i f_i\gamma_i$. However, if the value of Δq (resulting from the same change in shape) is sufficiently negative, then the final value of $q\sum_i f_i\gamma_i$ may be lowered. This effect is usually very slight (whereas the effect of σ_i is more significant), and is most prevalent when the values of γ_i are similar and the nanocrystals are very small. As the nanocrystal size increases, the value of Δq decreases and the effect of Δf_i dominates, eventually making this type of shape variation energetically unfavorable (i.e., converging to the Wulff shape). We can see such a variation in Figure 1, where the shape is defined in terms of the fraction of {111} surface area. Although visually the shape appears to change very little, we can see that small pyrite nanocrystals have ~50% {111} surface area, at ~5 nm in diameter we can expect a cuboctahedral shape (with ~37% {111} surface area), and at sizes >20 nm we can expect a truncated cube shape that converges rapidly to the Wulff shape with ~26% {111} surface area.

However, although the equilibrium shape of pyrite occupies the cuboctahedron-truncated cube shape-continuum (depending on size) it is possible that other shapes may be formed kinetically. For example, pyrite macrocrystals are often found to adopt perfect cubic morphologies, and unusual decahedral morphologies with pentagonal facets, known as pyritohedrons. Since pyrite nanostructures are rarely formed under equilibrium conditions, it is therefore reasonable to assume that such shapes are equally plausible at the nanoscale; formed as a result of natural (or synthetic) templating, or kinetically due to certain environmental factors influencing the growth rates on different facets. Nevertheless, once formed, some nonequilibrium shapes will still be more stable than others. To investigate this issue, a collection of possible shapes have been considered, by including only limited subsets of crystallographic forms (and therefore γ_i and σ_i), as shown in Figure 2. Among these shapes are the perfect closed forms of the cube (Figure 2a), octahedron (Figure 2c), dodecahedron (Figure 2e), and pyritohedron (Figure 2g), enclosed entirely by {100}, {111}, {110}, and {210} surfaces, respectively. In addition to this we have included the optimized shape (Figure 2b) as described above, a modified

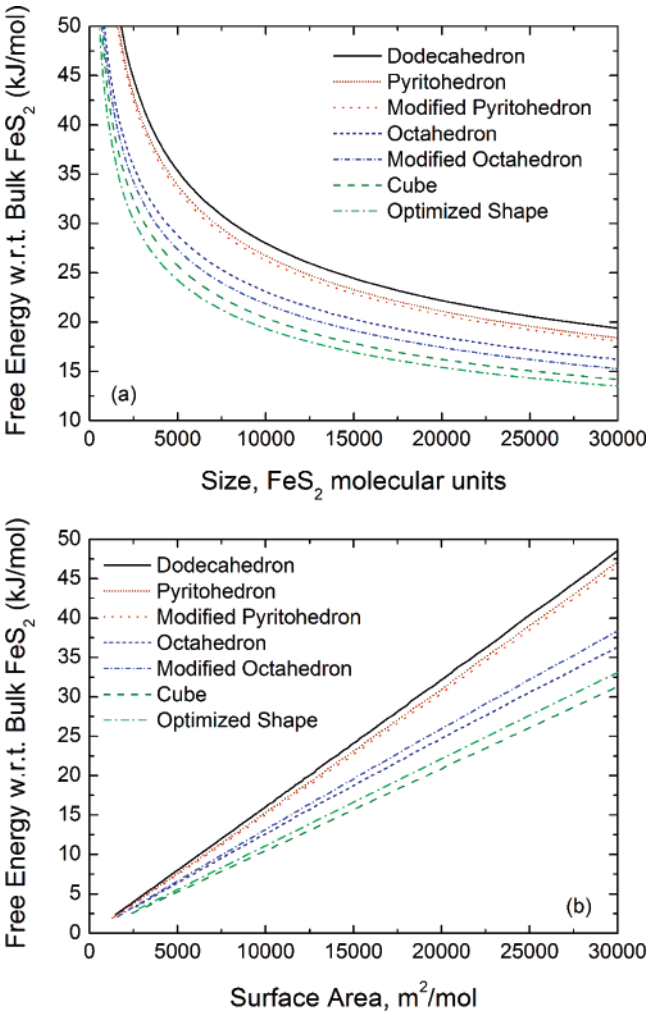

Figure 3. Free energy of formation for pyrite FeS_2 nanocrystals with a variety of shapes, with respect to bulk pyrite, (a) as a function of the number of molecular units (or total volume) and (b) as a function of the surface area.

octahedron enclosed by {111} and {210} facets (Figure 2d), and a modified pyritohedron enclosed by {210} and {110} facets (Figure 2f).

The free energy of formation G with respect to bulk pyrite has then been calculated for each of the shapes shown in Figure 2. These results are shown in Figure 3a, as a function of the number of FeS_2 molecular units, which is a measure of the total volume. This figure shows that the energetic ordering of the shapes as follows: optimized shape < cube < modified octahedron < octahedron < modified pyritohedron < pyritohedron < dodecahedron. The energetic ordering of the perfect closed forms (cube < octahedron < pyritohedron < dodecahedron) is consistent with the ordering of the respective surface energies. In each case the modifications of these shapes lowers the free energy of formation, even though higher energy facets are introduced, due to more favorable surface-to-volume ratios (q). These modified shapes are effectively more "spherical".

In general, there is also a distinct energetic separation between the shapes dominated by {100} and/or {111} facets, and those dominated by {110} and/or {210} facets. This indicates that, although nonequilibrium shapes may be formed during intentional (and unintentional) nonequilibrium synthesis, pyritohedrons or dodecahedral shapes are less likely to occur at small sizes. This is confirmed when we compare this collection of shapes as a function of surface area (see Figure 3b), as is often done during calorimetry studies of formation enthalpies.[52] Here

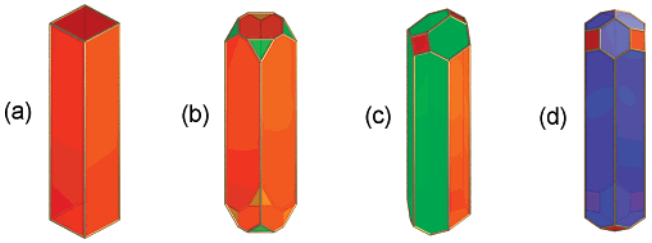

Figure 4. A collection of shapes for pyrite FeS_2 nanorods with different axial orientations, formed using limited combinations of crystallographic forms: (a) nanorod A in the ±[001] direction and (b) nanorod B in the ±[001] direction, (c) in the ±[011] direction, and (d) in the ±[111] direction. {100} facets are shown in red, {111} facets in green, and {110} facets in blue.

we see some reordering of the lower energy shapes, since shapes with equivalent surface area do not necessarily have the same volume, but we still observe the same energetic separation between the high- and low-energy morphologies. Note also how the shape can dramatically alter the slope of these results, a factor that is rarely taken into consideration during experimental studies.[52]

3.2. Nanorods and Nanowires. Looking instead to 1-D pyrite FeS_2 nanostructures, although it has been shown that the use of ethylenediamine during synthesis produces samples with rod-like morphology[25] with varying aspect ratio, it is not clear if these shapes are a thermodynamic or kinetic product, or if there is a preferred axial orientation as a function of size or degree of dimensional anisotropy. To investigate these issues we have used the shape-dependent model to calculate the free energy of formation for a collection of nanorods, as shown in Figure 4. This collection contains two different nanorods oriented in the ±[001] direction, denoted as A and B. These nanorods both have square cross-sections and differ only by the truncation of the corners in the {111} directions, as shown in Figure 4, parts a and b, respectively. In addition to this nanorods oriented in the ±[011] and ±[111] directions are also included (see Figure 4, parts c and d, respectively), both of which have hexagonal cross-sections.

As with the nanoparticles in section 3.1, the free energy of formation (with respect to bulk pyrite) has then been calculated for each of the shapes shown in Figure 4, as a function of size. These results are shown in Figure 5a, as a function of the number of FeS_2 molecular units, where we can see that there is a very close competition between ±[001] oriented and ±[011] oriented nanorods. This indicates that the formation of ±[001] or ±[011] oriented nanorods is likely to be kinetically driven. We can also see that the ±[001] or ±[011] oriented nanorods are considerably lower in free energy than the ±[111] oriented nanorod. This is significant, since pyrite nanorods grown experimentally have been found have axes in the ±[111] direction.[25] It is likely that, given the large energetic separation between the axial orientations, the growth directions are influenced by more than simply growth kinetics. Our results therefore support the assumption that the ethylenediamine used during synthesis (in addition to inducing 1-D growth) is also influential in determining the axial orientation, and suggest that other solvents or surfactants would promote growth along ±[001] or ±[011].

It is important to point out that the results shown in Figure 5a are "aspect conserving", with a constant aspect ratio of 10. Since as-grown pyrite nanorods present a variety of lengths and aspect ratios, we have also calculated the free energy of formation for each of the shapes shown in Figure 4, as a function of aspect ratio and length. These results are shown in Figure 5, parts b and c, respectively, depending upon whether the total

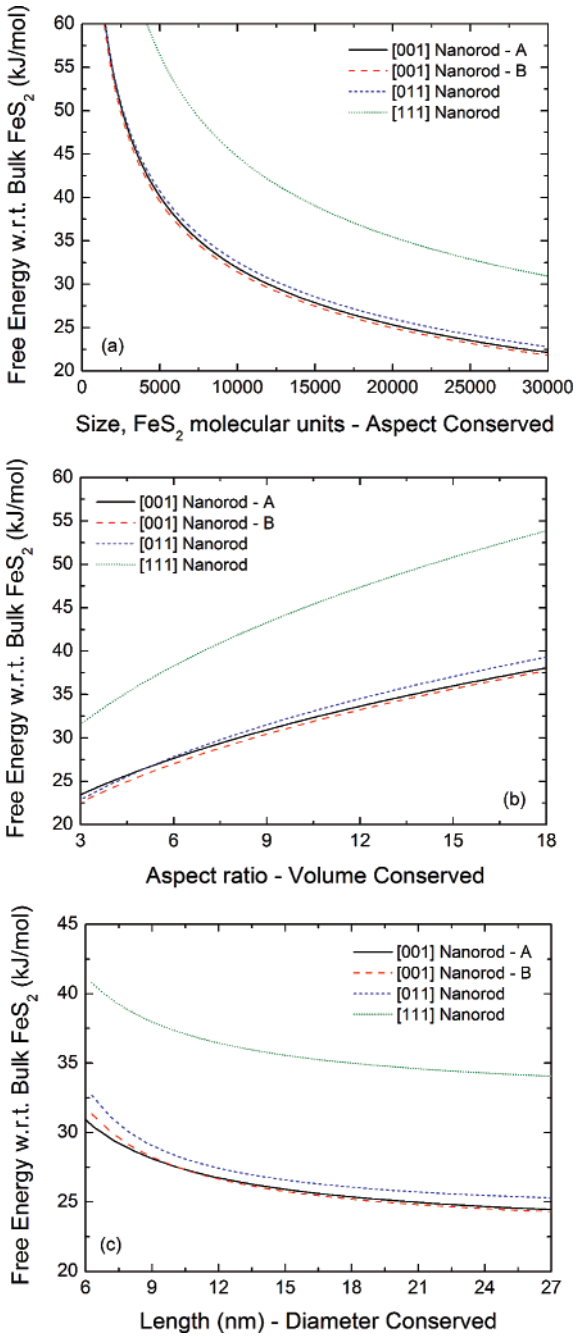

Figure 5. Free energy of formation for pyrite FeS_2 nanorods of different axial orientations, with respect to bulk pyrite, (a) as a function of the number of molecular units (or total volume), (b) as a function of the aspect ratio, and (c) as a function of the total length.

volume has been conserved. In the case of Figure 5b, the total volume has been conserved at 10^4 FeS_2 molecular units, so that the change in aspect ratio may be thought of as a type of deformation (where extension along the axis is accompanied by a reduction of the diameter). We can see here that, for the same total volume, 1-D nanostructures are less favorable than 0-D nanostructures, suggesting that we would expect a reduction in aspect ratio (a morphological transformation) given a suitable driving force (such as during annealing). In the case of Figure 5c, the diameter has been conserved at 5 nm, so that the change in aspect may be thought of as growth along the corresponding axes. We can see here that, if the increase in mass is restricted to the growth/axial direction, the formation of 1-D nanostruc-

tures is energetically favorable. This suggests that nanorod and nanowire formation is preceeded by the formation of quasi-spherical nanocrystal 'seeds' and that the growth rate perpendicular to the eventual axis is very small compared to that in the axial direction. This explains the very high aspects observed by Xuefeng et al.[25] and later by Kar and Chaudhuri,[29] and is consistent with observations of the early stages of formation of CdSe quantum wires.[34,53]

4. Conclusion

Therefore, by using a shape-dependent thermodynamic model, and energetic and elastic parameters calculated from first principles, we have examined the morphological stability of pyrite nanocrystals and nanorods, over a range of sizes and aspect ratios. Our results indicate that pyrite nanocrystals are likely to be dominated by cuboctahedral to truncated-cubic morphologies, since shapes (such as the decahedral pyritohedron) featuring {210} and {110} facets are less energetically favorable, especially at small sizes. We have also shown that it is energetically unfavorable for pyrite nanorods to have ±[111] axes (when the surfaces are "clean"), suggesting that the use of ethylenediamine during synthesis may be responsible for the rapid growth along this direction, rather than the more favorable ±[001] or ±[011] directions.

Future work will be focused on examining the effect of surface chemistry on the shape of FeS_2 nanocrystals and nanorods, and the phase stability between the pyrite and the (*Pnnm*) marcasite phases.

Acknowledgment. This work has been supported by the Glasstone Benefaction at the University of Oxford. The authors would like to acknowledge the use of the Australian Partnership for Advanced Computing supercomputer center in carrying out this work.

References and Notes

(1) Ennaoui, A.; Tributsch, H. *Sol. Cells* **1984**, *13*, 197.
(2) Ennaoui, A.; Fiechter, S.; Goslowsky, H.; Tributsch, H. *J. Electrochem. Soc.* **1985**, *132*, 1579.
(3) Ennaoui, A.; Fiechter, S.; Jaegermann, W.; Tributsch, H. *J. Electrochem. Soc.* **1986**, *133*, 97.
(4) Wang, S. S.; Seefurth, R. N. *J. Electrochem. Soc.* **1987**, *134*, 530.
(5) Tributsch, H. *Struct. Bonding* **1982**, *49*, 128. Tributsch, H. In *Modern Aspects of Electrochemistry*; Bockris, J. O., Ed.; Pergamon: Oxford, UK, 1986; Vol. 14, Chapter 4.
(6) Bucher, E. *Appl. Phys.* **1978**, *17*, 1.
(7) Bither, T. A.; Bouchard, R. J.; Cloud, W. H.; Donohue, P. C.; Siemons, W. J. *Inorg. Chem.* **1968**, *7*, 2208.
(8) Birkholz, M.; Fiechter, S.; Hartmann, A.; Tributsch, H. *Phys. Rev. B* **1991**, *43*, 11926.
(9) Ennaoui, A.; Fiechter, S.; Pettenkofer, Ch.; Alonso-Vante, N.; Buker, K.; Bronold, M.; Hopfner, Ch.; Tributsch, H. *Sol. Energy Mater. Sol. Cells* **1993**, *29*, 289.
(10) Muscat, J.; Hung, A.; Russo, S.; Yarovsky, I. *Phys. Rev. B* **2002**, *65*, 054107.
(11) Chatzitheodrou, G.; Fiechter, S.; Kunst, M.; Jaegermann, W.; Tributsch, H. *Mater. Res. Bull.* **1986**, *21*, 1481.
(12) Chatzitheodrou, G.; Fiechter, S.; Kunst, M.; Luck, J.; Tributsch, H. *Mater. Res. Bull.* **1988**, *23*, 1261.
(13) Luck, J.; Hartmann, A.; Fiechter, S.; Fresen. Z. *Anal. Chem.* **1989**, *334*, 441.
(14) Braum, P. V.; Osenar, P.; Stupp, S. I. *Nature* **1996**, *380*, 325.
(15) Han, W. Q.; Fan, S. S.; Li, Q. Q.; Hu, Y. D. *Science* **1997**, *277*, 1287.
(16) Wang, S. S.; Joselevich, E.; Woolley, A. T.; Cheung, C. L.; Lieber, C. M. *Nature* **1998**, *394*, 52.
(17) Frank, S.; Poncharal, P.; Wang, Z. L.; Heer, W. A. *Science* **1998**, *280*, 1744.
(18) Lee, C. J.; Lee, T. J.; Lyu, S. C.; Zhang, Y.; Ruh, H.; Lee, H. J. *Appl. Phys. Lett.* **2002**, *81*, 3648.
(19) Li, Y. D.; Liao, H. W.; Ding, Y.; Qian, Y. T.; Yang, L.; Zhou, G. E. *Chem. Mater.* **1998**, *10*, 2301.
(20) Chen, X.; Hu, H.; Xu, N.; Zhao, F.; Lin, W.; Lin, G.; Fu, Y.; Huang, Z.; Wang, H.; Wu, M. *Inorg. Chem.* **2003**, *42*, 3100.
(21) Ma, C.; Moore, D.; Li, J.; Wang, Z. L. *Adv. Mater.* **2003**, *15*, 228.
(22) Jiang, Y.; Meng, X. M.; Liu, J.; Xie, Z. Y.; Lee, C. S.; Lee, S. T. *Adv. Mater.* **2003**, *15*, 323.
(23) Rao, C. N. R.; Deepak, F. L.; Gundiah, G.; Govindaraj, A. *Prog. Solid State Chem.* **2005**, *31*, 5.
(24) Zhou, T. Y.; Xin, X. Q. *Nanotechnology* **2004**, *15*, 534.
(25) Xuefeng, Q.; Yi, X.; Yitai, Q. *Mater. Lett.* **2001**, *48*, 109.
(26) Nath, M.; Choudhury, A.; Kundu, A.; Rao, C. N. R. *Adv. Mater.* **2003**, *15*, 2098.
(27) Yu, S. H.; Yang, J.; Han, Z. H.; Zhou, Y.; Yang, R. Y.; Qian, Y. T.; Zhang, Y. H. *J. Mater. Chem.* **1999**, *9*, 1283.
(28) Kar, S.; Chaudhuri, S. *Chem. Phys. Lett.* **2004**, *398*, 22.
(29) Kar, S.; Chaudhuri, S. *Mater. Lett.* **2005**, *59*, 289.
(30) José-Yacamán, M. *J. Comput. Theor. Nanosci.* **2007**, *4*, 195.
(31) Barnard, A. S.; Zapol, P. *J. Chem. Phys.* **2004**, *121*, 4276.
(32) Barnard, A. S.; Curtiss, L. A. *Nano Lett.* **2005**, *5*, 1261.
(33) Barnard, A. S.; Yeredla, R. R.; Xu, H. *Nanotechnology* **2006**, *17*, 3039.
(34) Barnard, A. S.; Xu, H.; Li, X.; Pradham, N.; Peng, X. *Nanotechnology* **2006**, *17*, 5707.
(35) Barnard, A. S. *J. Phys. Chem. B* **2006**, *110*, 24498.
(36) Perdew, J.; Wang, Y. *Phys. Rev. B* **1992**, *45*, 13244.
(37) Kresse, G.; Hafner, J. *Phys. Rev. B* **1993**, *47*, RC558.
(38) Kresse, G.; Hafner, J. *Phys. Rev. B* **1996**, *54*, 11169.
(39) Vanderbilt, D. *Phys. Rev. B* **1990**, *41*, 7892.
(40) Kresse, G.; Hafner, J. *J. Phys.*: *Condens. Matter* **1994**, *6*, 8245.
(41) Kresse, G.; Furthmüller, J. *Compos. Mater. Sci.* **1996**, *6*, 15.
(42) Wood, D. M.; Zunger, A. *J. Phys. A* **1985**, *18*, 1343.
(43) Raybaud, P.; Hafner, J.; Kresse, G.; Toulhout, H. *J. Phys.*: *Condens. Matter* **1997**, *9*, 11085.
(44) Finklea, S.; Cathey, L.; Amma, E. *Acta Crystallogr., Sect. A*: *Cryst. Phys. Diffr. Theor. Gen. Crystallogr.* **1976**, *32*, 529.
(45) Birch, F. *J. Geophys. Res.* **1987**, *83*, 1257.
(46) Drickamer, H. G.; Lynch, R. W.; Clendenen, R. L.; Perez-Albuerne, E. A. *Solid State Phys.* **1966**, *19*, 135.
(47) Fujii, T.; Yoshida, A.; Tanaka, K.; Marumo, F.; Noda, Y. *Mineral. J.* **1986**, *13*, 202.
(48) Jephcoat, A.; Olson, P. *Nature* **1987**, *325*, 332.
(49) Barnard, A. S.; Zapol, P. *Phys. Rev. B* **2004**, *70*, 235403.
(50) Hung, A.; Muscat, J.; Yarovsky, I.; Russo, S. *Surf. Sci.* **2002**, *513*, 511.
(51) Hung, A.; Muscat, J.; Yarovsky, I.; Russo, S. *Surf. Sci.* **2002**, *520*, 111.
(52) Deore, S.; Navrotsky, A. *Am. Mineral.* **2006**, *91*, 400.
(53) Pradhan, N.; Xu, H.; Peng, X. *Nano Lett.* **2006**, *6*, 720.